

Ion kinetic-energy distributions and Balmer-alpha (H_{α}) excitation in Ar- H_2 radio-frequency discharges

S. B. Radovanov,^{a)} J. K. Olthoff,^{b)} R. J. Van Brunt, and S. Djurović^{c)}
National Institute of Standards and Technology,^{d)} Gaithersburg, Maryland 20899

(Received 26 October 1994; accepted for publication 5 April 1995)

Excited neutrals and fast ions produced in a 13.56 MHz radio-frequency discharge in a 90% argon – 10% hydrogen gas mixture were investigated, respectively, by spatially and temporally resolved optical emission spectroscopy, and by mass-resolved measurements of ion kinetic energy distributions at the grounded electrode. The electrical characteristics of the discharge were also measured and comparisons are made with results obtained for discharges in pure H_2 under comparable conditions. Measurements of Balmer-alpha (H_{α}) emission show Doppler-broadened emission that is due to the excitation of fast atomic hydrogen neutrals formed from ion neutralization processes in the discharge. Temporally and spatially resolved emission profiles of the H_{α} radiation from the Ar- H_2 mixture are presented for the “slow” component produced predominately by electron-impact dissociative excitation of H_2 , and for the “fast” component corresponding to energies much greater than can be derived from dissociative excitation. For the Ar- H_2 mixture, the fast component is significantly enhanced relative to the slow component. The measured kinetic-energy distributions and fluxes of predominant ions in the Ar- H_2 mixture, such as H_3^+ , H_2^+ , H^+ , and ArH^+ , suggest mechanisms for the formation of fast hydrogen atoms. The interpretation of results indicate that H^+ and/or H_3^+ , neutralized and backscattered by collision with the powered electrode, are the likely sources of fast hydrogen atoms that produce Doppler-shifted H_{α} emission in the discharge. There is also evidence at the highest pressures and voltages of “runaway” H^+ ions formed near the powered electrode, and detected with kinetic energies exceeding 100 eV at the grounded electrode.

I. INTRODUCTION

Radio-frequency (rf) discharges produced in argon-hydrogen mixtures are useful for surface cleaning applications,¹ while discharges involving mixtures of argon, hydrogen, and methane have been used for etching of GaAs wafers.² An understanding of these processes requires a knowledge of the role of collisions of ions and energetic neutrals with surfaces and other particles in the plasma. Particularly, in collision dominated discharges, ion and neutral transport in the sheath region are important in determining the discharge-surface interactions.

In addition to industrial applications, ion transport in Ar- H_2 gas mixtures has been considered as a prototype system for experimental investigations and rigorous quantum-theoretical studies.^{3–10} A recent review article on state-selected and state-to-state cross-section measurements for several ion-molecule reaction systems shows that an increasing interest has been paid to the Ar- H_2 system.¹¹

Few investigations in Ar- H_2 mixtures have been performed in low pressure dc^{12–14} or rf¹⁵ discharges. A recent optical emission study¹⁵ of an Ar- H_2 mixture in 13.56 MHz rf glow discharges shows an increase in Doppler-broadened Balmer-alpha (H_{α} , $\lambda = 656.3$ nm) emission when argon is

added to a hydrogen discharge. The observed Doppler broadened profiles have a wide component which corresponds to emission from hydrogen atoms with kinetic energies approaching 100 eV. The study of hydrogen excitation in Ar- H_2 mixtures in dc low-current discharges¹² has also shown that the presence of argon atoms plays a significant role in producing a large increase in the H_{α} emission. These studies indicate the significance of the excitation of atoms by collisions, and the interactions of fast ions and neutrals with the electrode surface. The importance of fast neutrals is well recognized primarily because they are sources of secondary electrons and of sputtering at the electrode surfaces.

The identity and kinetic energy distribution of ions, along with their role in producing fast neutrals, has not been thoroughly investigated for rf glow discharges generated in mixtures of argon and hydrogen. Kinetic energy distributions of Ar^+ and various ions from hydrogen in an Ar(69%)- H_2 (31%) mixture were determined from simulations by Field *et al.*¹⁶ for comparison with experimentally obtained energy distributions at the powered electrode of rf discharges¹⁷ for collisionless, low pressure (0.4 Pa) conditions. Also an experimental study of the kinetic-energy distributions at the powered electrode of a 13.56 MHz rf discharge in a similar Ar- H_2 mixture was made by A. Manenschijn *et al.*¹⁸ without mass analysis. However, the interpretation of these data is hampered by lack of knowledge about the identity of the ions, and does not address the collisional processes that dominate at higher pressures.

In order to more fully understand the origin of fast neutrals in Ar- H_2 rf discharges, and to determine the role that

^{a)}Present address: Department of Chemical and Nuclear Engineering, University of New Mexico, Albuquerque, NM 87131.

^{b)}Electronic mail: olthoff@eeel.nist.gov

^{c)}Permanent address: Institute of Physics, Novi Sad, Trg Dositja Obradivca 4, 21000 Novi Sad, Yugoslavia.

^{d)}Electricity Division, Electronics and Electrical Engineering Laboratory, Technology Administration, U.S. Department of Commerce.

fast ions play in their production, we have carried out a detailed experimental investigation of positive ion production and transport in Ar-H₂ rf discharges in conjunction with simultaneous optical and electrical measurements. Since fast neutrals most probably originate, directly or indirectly, from collisions of energetic ions with neutral particles or surfaces, one objective of this work was to determine the kinetic-energy distributions of ions formed in the discharge, such as H⁺, H₂⁺, H₃⁺, ArH⁺, Ar⁺ and Ar⁺⁺. This was a part of a wider study of rf glow discharges in mixtures of argon and other gases as used in various applications.¹⁹ By measuring kinetic energies of mass-identified ions striking the grounded electrode of a parallel-plate reactor it was possible to determine the dominant ion species present in the discharge and to infer the most likely ion formation processes for each species.

The experimental techniques chosen to analyze the emission were measurements of the temporal and spatial dependence of the fast and slow component of the Doppler-broadened H_α emission. Correlations among the measured ion kinetic-energy distributions (IEDs), current and voltage waveforms (phase and amplitude), and Doppler-broadened H_α emission are examined.

While investigations of Ar-H₂ discharges are few, there are numerous investigations of dc and rf discharges in pure hydrogen.^{20,21} A recent publication²² provides an explanation of the contribution of surface reflection to the excitation of fast hydrogen atoms in low-pressure dc hydrogen discharges. These authors were the first to report that backscattered fast H atoms, from incident H, H⁺, H₂, and H₂⁺ and subsequent excitation by collisions with H₂, are responsible for most of the H_α emission in the cathode fall region of low current, uniform-field (Townsend) discharges in H₂. Similarities between these observations for a dc discharge and observations made here under rf conditions are explored.

II. EXPERIMENT

All discharges investigated in these experiments were generated in a Gaseous Electronic Conference (GEC) rf Reference Cell described previously.²³ The reactor consists of two 10.2 cm, parallel-plate electrodes separated by 2.5 cm. Mixtures of ultra-high purity argon and hydrogen gases were supplied to the cell through a showerhead arrangement of small holes in the lower electrode. The total flow was maintained at 1.7×10^{-2} Pa m³/s (10 sccm). Except where specifically noted, all data presented here are for a 10% H₂ / 90% Ar gas mixture. Optical data were usually taken at 13.3 Pa, while ion energy data were obtained at four different pressures 1.3, 4.0, 13.3, and 33.3 Pa (10, 30, 100, and 250 mTorr).

The stainless steel upper electrode is grounded to the vacuum chamber and the lower aluminum electrode is capacitively-coupled to a 13.56 MHz power supply. More details of the electrical configuration of the cell, including the shunt circuitry and filter box, are described elsewhere.²³⁻²⁵ The current and voltage waveforms were measured near the base of the powered electrode, and the

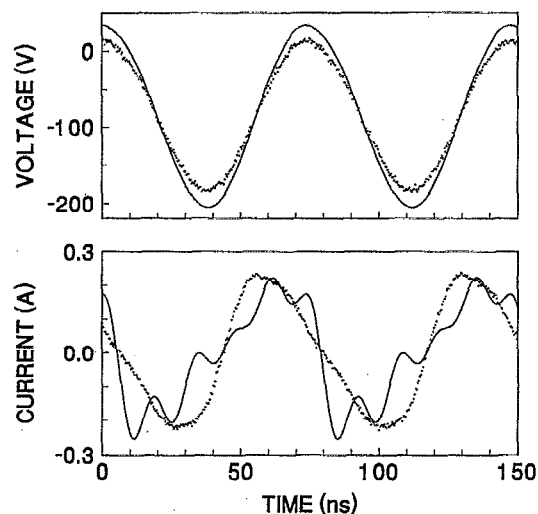


FIG. 1. Voltage and current waveforms measured for an Ar-H₂(10%) discharge at $p = 13.3$ Pa and $V_{pp} = 200$ V. The dotted curves are the measured waveforms, while the solid curves represent the waveforms at the powered electrode as calculated by an equivalent circuit model (see Ref. 24).

applied peak-to-peak rf voltage (V_{pp}) in these experiments was maintained at 200 V.

Ions from the discharge were sampled through an 0.1 mm aperture in the grounded electrode. The grounded electrode was made of polished stainless steel in order to reduce the effect of surface charging on the measured kinetic-energy distributions of the sampled ions.²⁶ The aperture acts as the inlet to an electrostatic ion energy analyzer (ESA) coupled to a quadrupole mass spectrometer (QMS). Kinetic-energy distributions of positive ions were measured by setting the quadrupole to a particular mass-to-charge ratio (m/z), and then scanning the energy of the ions transmitted through the ESA. The resolution of the energy analyzer was determined to be 1.5 eV (full width at half maximum) with an uncertainty in the measured ion energy scale of ± 1 eV. The resolution of the QMS was approximately 0.5 u (full width at half maximum). All data were obtained with the same analyzer settings to allow comparison of the intensities of different ion signals. Our earlier measurements²⁷ have shown that the kinetic-energy distributions of ions are reproducible under a given set of operating conditions, but that signals for low-energy ions (below 5 eV) are subject to discrimination which may significantly affect the observed relative ion fluxes. Placing the ion sampling orifice in a clean stainless steel electrode considerably reduces this low energy discrimination.²⁶

Spectral scans from the discharge were obtained using a scanning monochromator having a reciprocal dispersion of 0.416 nm/mm, and a cooled photomultiplier with nearly constant radiant sensitivity from 250 to 820 nm. Optical emission versus axial position scans were obtained by focusing the light on the entrance slit of the monochromator and scanning the discharge region between the electrodes. All data presented here were obtained by observing the emission at 90° from the central axis of the electrodes, i.e. parallel to the electrode surfaces. Other data not shown were obtained at an

TABLE I. Amplitudes of the fundamental Fourier components at the powered electrode of the voltage (V_1) and current (I_1) waveforms, the phase (ϕ_1) of the voltage relative to the current, the dc self-bias potential (V_b), and the power dissipated in a discharge as a function of the gas mixture for $V_{pp}=200$ V and $p=13.3$ Pa.

Gas	V_1 (V)	I_1 (mA)	ϕ_1 (°)	V_b (V)	Power (W)
H ₂	120.0	92.5	-72.7	-70.5	1.6
Ar-H ₂ (90%)	120.2	102.3	-73.6	-70.7	1.7
Ar-H ₂ (10%)	120.0	180.8	-77.4	-80.9	2.4
Ar	122.5	224.5	-81.55	-94.6	2.0

angle of observation of 80°. Phase-resolved measurements of the H α emission were obtained by utilizing a time-to-amplitude converter (TAC) and multichannel analyzer (MCA). The start signal is generated at a fixed point on the rf voltage waveform, and the TAC is stopped by a photon-initiated pulse from the photomultiplier system. The data are accumulated in the MCA as 256 channels with a time resolution of 0.78 ns/channel. Further details of the optical apparatus including determination of the instrumental signal delays are given elsewhere.²⁸

III. RESULTS

A. Electrical measurements

An example of the voltage and current waveforms for a discharge in the Ar-H₂(10%) mixture, with $V_{pp}=200$ V and a pressure of 13.3 Pa, are shown in Fig. 1. Both waveforms were obtained by digitizing the probe signals (dotted curve) and then fitting and correcting for probe time delays and cell parasitics (full curve). These curves are correlated with the time-resolved optical emission data presented later. Further analysis of the electrical measurements is performed by calculating the fundamental Fourier components of the voltage and current waveforms, the phases of the impedance, the magnitude of the dc self-bias potential and the power dissipated in the discharge.^{23,24} These values are given in Table I for several Ar-H₂ mixtures ranging from pure hydrogen to pure argon, and are similar to those published previously for pure argon.^{23,27,28} From Table I one can see that as hydrogen is added to argon, lower current amplitudes are observed and the phase of the voltage relative to the current shifts towards zero. The decrease of the amplitude of the fundamental current component with increasing hydrogen concentration can

TABLE II. Amplitudes of the fundamental Fourier components at the powered electrode of the voltage (V_1) and current (I_1) waveforms, the phase (ϕ_1) of the voltage relative to the current, the dc self-bias potential (V_b), and the power dissipated for rf discharges in a 90% Ar - 10% H₂ gas mixture with $V_{pp}=200$ V as a function of pressure.

Pressure (Pa)	V_1 (V)	I_1 (mA)	ϕ_1 (°)	V_b (V)	Power (W)
1.3	121.3	109.1	-78.7	-95.1	1.3
4.0	120.3	138.5	-79.4	-93.3	1.5
13.3	121.6	196.3	-77.8	-84.7	2.5
33.3	121.6	268.8	-74.9	-71.5	4.3

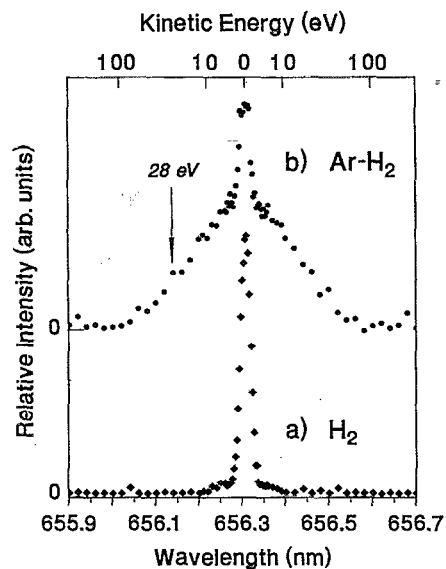


FIG. 2. Balmer-alpha emission profiles observed perpendicular to the electrode axis of a low pressure rf discharge in (a) H₂ and (b) Ar-H₂(10%) at 13.3 Pa and $V_{pp}=200$ V, at a distance of 1.5 mm from the grounded electrode.

be understood from the decrease in electron density, sheath capacitance, and displacement current that occur with the addition of hydrogen, as discussed later. Table II shows the same parameters but for four different pressures in the Ar-H₂(10%) mixture that were used while obtaining the ion energy data. The current (I_1) and power are observed to increase with increasing pressure, while the magnitude of the self bias voltage (V_b) decreases. Again, the magnitude of the electrical values presented in Table II are similar to those published for pure argon discharges,^{23,27,28} thus indicating that the small amount (10%) of added hydrogen does not dramatically affect the bulk parameters of the argon discharge.

B. Time-averaged optical measurements

Representative time-averaged spectral profiles of the H α radiation, corresponding to the hydrogen atomic transition from the $n=3$ to $n=2$ level ($\lambda=656.3$ nm), emitted from rf discharges in pure H₂ and in the Ar-H₂ mixture are shown in Figs. 2(a) and 2(b), respectively. The broad components of the Balmer-alpha line, that manifest themselves as minor wings in the pure hydrogen spectrum and as much larger wings for the mixture, are due to Doppler broadening of the emission from fast hydrogen atoms. The corresponding kinetic energy of the hydrogen atoms is shown on the upper axis of Fig. 2.

The structure of the H α line emission from the pure H₂ discharge shows a slow component with an average energy of $\epsilon=0.2$ eV and a broadened component with $\epsilon=8.0$ eV which forms a narrow plateau. Similar structure has been reported by other researchers.²⁰ The thermal energy, or slow component of the line profile, which can be approximated by a Gaussian function, dominates in the pure hydrogen rf discharge with a gas pressure of $p=13.3$ Pa and $V_{pp}=200$ V.

According to beam experiments,²⁹⁻³³ the slow atoms in $n \geq 2$ states result from electron-impact excitation of singly bound ($1s\sigma_g$) ($n\lambda$) states of H_2 . The component in Fig. 2(a) corresponding to energies up to 8 eV is known²⁰ to result from dissociative ionization of hydrogen molecules. This plateau structure includes contributions from excitation to Rydberg states converging to the $2^2\Sigma_u^+$ ($2\pi\sigma_u$) ionic states. When the peak-to-peak voltage is increased to 300 V, an enhancement of this more energetic group of atoms can be observed in the region near the sheath boundary where the efficiency of the electronic collisions is greatest.

Doppler broadening due to this mechanism also occurs in the Ar- H_2 mixture, but is obscured by a much larger Doppler-broadened emission that is the result of fast H atoms (up to 100 eV) that must be formed by processes other than electronic excitation of H_2 , e.g., by collisions of fast atoms or ions with thermal molecules or surfaces.¹⁵ The fast component of this profile [see Fig. 2(b)] corresponds to translational kinetic-energies that are much higher than can be produced by electron-impact dissociative excitation or ionization of hydrogen molecules. While the time-averaged profiles in Fig. 2(b) are measured in the sheath region 1.5 mm from the grounded electrode, the widths of the fast and slow components of these profiles are observed to be similar throughout the whole interelectrode region of the discharge, over a wide range of gas pressures, applied rf voltages, and hydrogen concentrations in Ar- H_2 mixtures.¹⁵ Only the relative amplitudes of the fast and slow components vary with position. The calculated intensity ratios indicate that fast H($n=3$) atom densities exceed H($n=3$) atoms with thermal energies in the mixture at all positions in the discharge except for the bulk region where the number densities of fast to slow are comparable. The short atomic lifetime (15 ns) for the $n=3$ state of hydrogen suggests excitation and subsequent emission from fast atoms must be due to collisions that occur close to the observation point. The source and excitation mechanisms of the fast H atoms will be considered below.

For the remainder of this paper "slow" atoms are defined as H atoms with thermal energies (~ 0.2 eV), "intermediate" atoms have energies of 8-10 eV, and "fast" atoms have energies greater than 10 eV.

The observed dependence of H_α emission on distance along the axis measured from the grounded electrode (d) is shown in Fig. 3(a). Shown are data for both the slow and fast H atoms in an Ar- H_2 discharge. The results were obtained by scanning the observation point between the electrodes with the monochromator set at a given wavelength, in this case at the peak maximum (656.3 nm) and at 656.14 nm. The signal at 656.14 nm is on the wing of the spectral profile, and corresponds to a Doppler shift ($\Delta\lambda$) of 0.16 nm associated with hydrogen atoms that have kinetic energy greater than 28 eV. The spatial dependence of the slow component [Fig. 3(a) full curve] was determined by subtracting that portion of the emission due to fast atoms from the spectral profile. While the magnitude of the emission from fast hydrogen atoms with $\epsilon=28$ eV (dashed curve) can be compared with the emission from slow H atoms in this figure, the ratio of fast-to-slow atoms requires an integration over the spectral line-

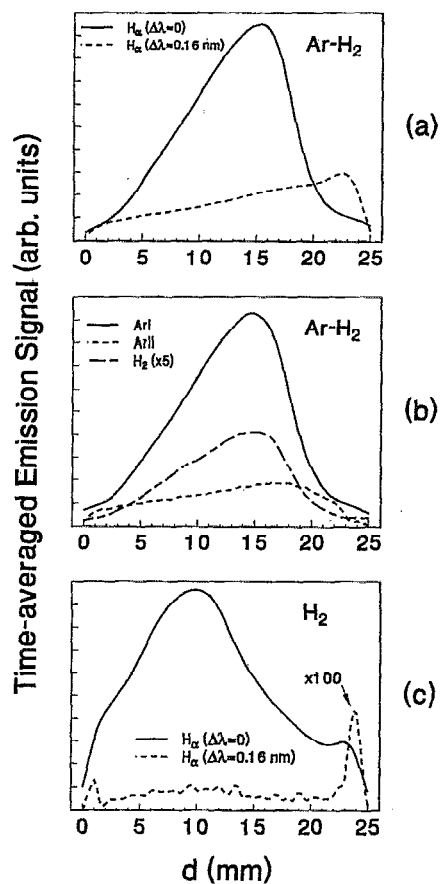


FIG. 3. Spatial dependence of time-averaged emission intensity from atomic and molecular species in Ar- H_2 (10%) (a) and (b); and in pure H_2 (c) discharges for the same conditions as Fig. 1. (a) The solid curve shows H_α emission (656.3 nm) from slow H($n=3$) atoms, and the dashed curve represents Doppler-shifted emission from fast H($n=3$) atoms. (b) The solid curve shows Ar I (425.9 nm) emission, the dashed curve displays Ar II (427.7 nm) emission, and the alternating-dashed curve is the 463.4 nm emission from a H_2 molecular line (the transition being $G^1\Sigma_g^+ - B^1\Sigma_u^+$). (c) The solid curve represents slow H($n=3$) atoms and dashed curve fast H($n=3$) atoms in pure H_2 discharge.

shape and has been presented elsewhere.¹⁵ The fast component shows a maximum of strong emission near the powered electrode, exceeding that from slow atoms, and a nearly linear decay as a function of distance from the powered electrode.

In contrast to the emission from fast atoms, the spatial dependence of the slow component peaks inside the plasma volume, well away from the electrodes. The distance from the peak emission to the powered electrode surface is representative of the time-averaged sheath width in the plasma, and shows that the fast emission component actually peaks inside the sheath region. Spatial profiles of other emission lines, such as a H_2 molecular line (long dashed curve), and argon ionic and atomic lines are shown in Fig. 3(b) to further characterize the discharge. The Ar I and Ar II spatial profiles are similar in shape to those measured previously²⁸ in pure argon, except that the peak emission is approximately 3 mm further from the powered electrode in the mixture, indicating an increase in sheath width with the addition of H_2 to argon.

The spatial profile of the H_2 molecular line, the Ar I line, and the "slow" H_α line, all of which are determined primarily by electron excitation rates, exhibit a maximum in approximately the same locations in the bulk of the discharge. The location of the emission maxima for the slow group of hydrogen and argon atoms undoubtedly corresponds to the region of the discharge where the electron density is highest.

For comparison, the spatial dependence of emission from slow and fast $H(n=3)$ in a pure hydrogen rf discharge are shown in Fig. 3(c). As in the mixture, the slow component (full curve) extends throughout the entire volume and peaks in the bulk of the discharge, although in this case the peak occurs 5 mm further from the powered electrode than for the mixture. The fast component of the H_α emission in pure hydrogen is much weaker than the slow component (note the $\times 100$ multiplication factor in the figure), and is primarily localized in a narrow luminous layer close to the electrode surfaces. This is consistent with fast H atom formation and excitation predominately near the electrode surfaces. The emission from fast H is not expected to extend significantly into the bulk of an H_2 discharge because of the quenching of $H(n=3)$ by collisions with H_2 .²⁰

C. Phase-resolved measurements

In addition to the time-averaged spatial dependence of H_α emission shown in Fig. 3(a), we also measured the phase-resolved optical emission from Ar- H_2 discharges. The time (phase) dependent emission by (a) fast $H(n=3)$ atoms ($\epsilon \geq 28$ eV), (b) slow $H(n=3)$, and (c) argon ions are shown in Fig. 4. Emission from two complete rf cycles are displayed to help differentiate statistically significant features from fluctuations due to noise. The emission maxima for the fast component occur approximately 1.5 mm from the surface of the powered electrode, in agreement with the time-averaged data shown in Fig. 3. The optical signal for fast $H(n=3)$ near the powered electrode exhibits a sinusoidal form nearly in phase with the applied voltage. Further from the powered electrode a significant signal is observed, but with no discernible phase dependence. The small signal fluctuations observed in the bulk of the discharge are not repeated in both rf periods and therefore can be attributed to noise.

The spatiotemporal profile for the slow $H(n=3)$ component [Fig. 4(b)] peaks 30 ns later in the rf cycle than the fast component, which places it near the applied voltage minimum. The time-varying component of the emission from slow H is observed to extend further into the bulk region than observed for the fast component. These observed differences between Figs. 4(a) and 4(b) in spatial location of the peak emission, spatial extent of the emission, and temporal phases are consistent with different excitation mechanisms for the fast and slow H atoms in the discharge.

The spatiotemporal profile of an Ar^+ emission line is shown in Fig. 4(c) for comparison, and is nearly identical with previous observations of ArII emission in rf discharges in pure argon,²⁸ again suggesting that the bulk of the discharge behaves predominately like a pure argon discharge. The peak emission for ArII occurs nearly 25 ns after the peak

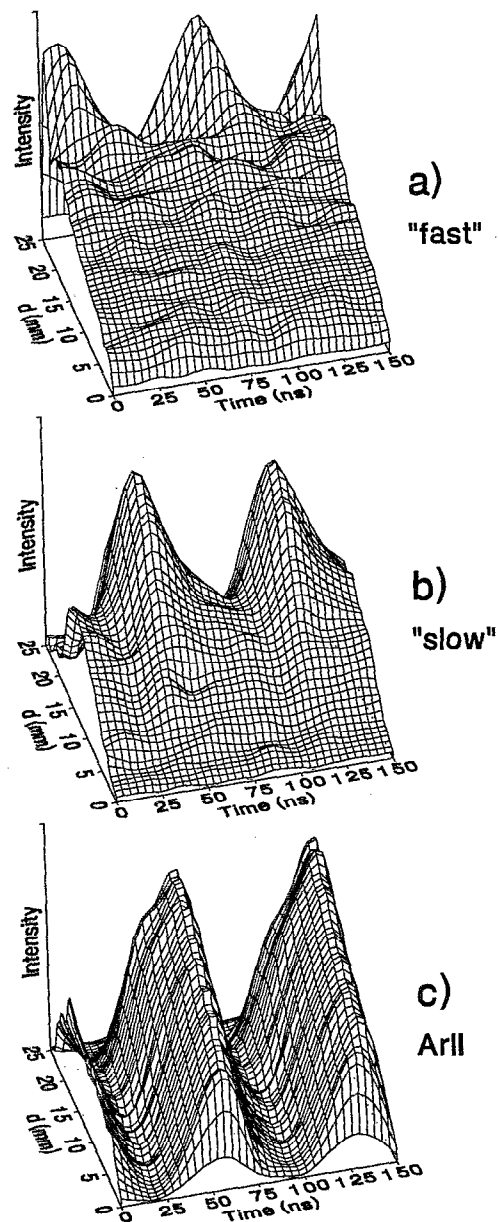


FIG. 4. Spatiotemporal profile of (a) Doppler-shifted H_α emission at 656.46 nm ($\Delta\lambda=0.16$ nm), (b) H_α emission at 656.30 nm, and (c) Ar II emission (427.7 nm) in an Ar- H_2 (10%) discharge for the same conditions as Fig. 1. The time scale (phase) is the same as in Fig. 1, i.e., $t=0$ corresponds to the maximum of the applied rf voltage, and d is the distance from the grounded electrode.

emission for the slow component in Fig. 4(b). The threshold for Ar^+ excitation is 25 eV, compared with 12 eV for H_α excitation, so the ArII emission is peaked later in the rf cycle, just after the time when the largest electric field is present in the powered sheath that accelerates the electrons to the energies required for the observed ionization and excitation.

D. Ion kinetic-energy distributions

Mass-resolved ion kinetic-energy distributions (IEDs) at the grounded electrode for discharges in the Ar- H_2 (10%) gas mixture were measured in order to identify ions that may be

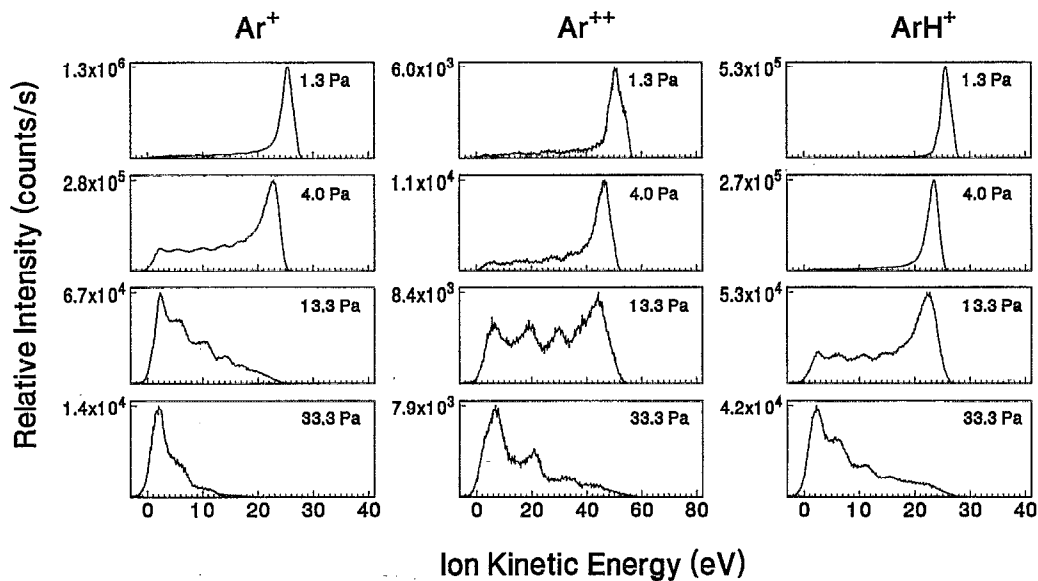


FIG. 5. Kinetic-energy distributions (relative ion intensity versus ion energy) of Ar^+ , Ar^{++} , and ArH^+ sampled from $\text{Ar-H}_2(10\%)$ rf discharges at various pressures with $V_{pp}=200$ V.

precursors to the fast H-atom formation responsible for the observed Doppler-broadened H_α emission. Discharge conditions ranged from low pressure (1.3 Pa) collisionless conditions, to higher pressures (33.3 Pa) where collisions in the sheath significantly affect ion transport through the sheaths. Unless otherwise specified the applied peak-to-peak voltage was held at 200 V for the data presented here.

The measured IEDs for Ar^+ , Ar^{++} , and ArH^+ are shown in Fig. 5 for the indicated gas pressures. The fluxes of ArH^+ and Ar^{++} striking the grounded electrode are small relative to the Ar^+ flux at the lower pressures, but become comparable to Ar^+ at 33.3 Pa. Under low-pressure, collisionless conditions, the IEDs for all three ions exhibit a single peak indicating that they are formed predominantly in the bulk of the discharge.³⁴ The mean kinetic energies of the ions decrease as the pressure in the discharge increases due to the increased probability of collisions. As in a pure argon discharge, symmetric charge-exchange in the sheath has a large influence on the IEDs for Ar^+ at the higher pressures and is responsible for secondary structure or "maxima" observed at energies below 20 eV.^{27,35} Similar secondary structure is observed for ArH^+ and Ar^{++} indicating that these ions can also be formed by collisions in the sheath region of the discharge.

The shapes and trends of the IEDs for the ions shown in Fig. 5 from the $\text{Ar-H}_2(10\%)$ discharge, are qualitatively similar to those obtained previously in pure argon.²⁷ The largest differences in the shapes of the IEDs for the mixture as compared to those in pure argon are evident at low energies, where a significantly higher signal is observed at energies below 10 eV. This can be explained by the use of a stainless-steel grounded electrode in place of an aluminum electrode on which the sampling orifice is located, as discussed in the experimental section and elsewhere.²⁶

The IEDs of the primary ions from hydrogen, H^+ , H_2^+ , and H_3^+ , are shown in Fig. 6 as a function of pressure. The magnitudes of the signal for these ions are comparable to those for the argon ions in Fig. 5 and therefore contribute significantly to the transport of the charge in the sheath region. The IEDs at 1.33 Pa correspond primarily to ions which have not experienced collisions in the sheath region. The appearance of a double-peak "saddle structure" in the IEDs of all three hydrogen ions is caused by modulation of the ion acceleration in the time dependent rf electric field.³⁶ This type of rf modulation of the IEDs is not observed for the heavier ions that contain argon (see Fig. 5) because of their longer transit times across the sheath. At higher pressures the IEDs are influenced by collisions with argon atoms and hydrogen molecules, resulting in lowering of the mean energy as also observed for the argon-containing ions. In general, the reduction in mean energies with increasing pressure is less pronounced for the ions containing hydrogen (Fig. 6), compared to Ar^+ and Ar^{++} shown in Fig. 5. This is most likely due to the less significant effect of symmetric charge-transfer collisions due to the lower H_2 concentration.

From Figs. 5 and 6 it is apparent that H_3^+ exhibits the highest mean kinetic energy of all the ions, while H^+ exhibits the largest maximum kinetic energy of any H-containing ion in the discharge. In fact, at pressures greater than 4 Pa, the IEDs shown in Fig. 6 indicate that H^+ ions are present at the grounded electrode with kinetic energies exceeding 40 eV.

Figure 7 shows a semi-log plot of two H^+ IEDs over a much larger range of kinetic energies. For the conditions at which the optical data were obtained ($V_{pp}=200$ V and $p=13.3$ Pa), a weak H^+ ion signal is detected up to nearly 100 eV, which is similar to the maximum kinetic energy of H

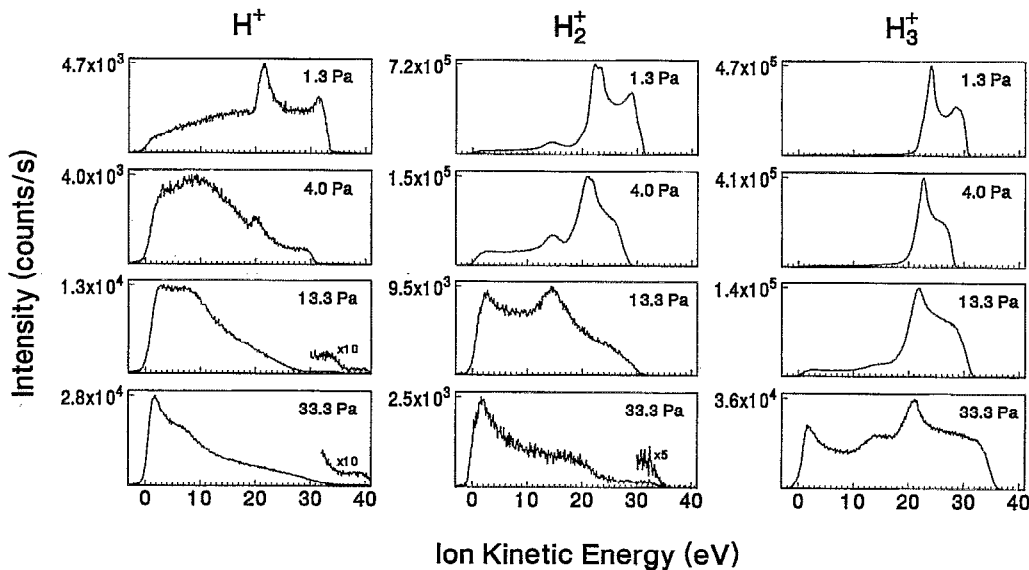


FIG. 6. Kinetic-energy distributions of H^+ , H_2^+ , and H_3^+ in Ar- H_2 (10%) rf discharges for the same conditions as Fig. 5.

atoms that is detected by Doppler-shift spectroscopy in Fig. 2. As the pressure and applied voltage are increased to 33.3 Pa and 350 V, respectively, the intensity of the high energy tail is observed to increase until the IED clearly extends beyond 100 eV (the maximum kinetic energy detectable with our energy analyzer). These high energy ions are an indication of conditions suitable for the formation of “runaway” ions,³⁷ i.e., ions with sufficiently high energy so that the cross section for collisions resulting in significant loss of energy are very small. The implications of runaway ions will be discussed in Section IV.

By integrating the IEDs shown in Figs. 5 and 6, it is possible to estimate the relative fluxes of the ions for each set of plasma conditions. The results of these calculations are presented in Fig. 8 for the Ar- H_2 (10%) mixture as a function of pressure. The vertical dotted line indicates the conditions under which the optical data presented in Figs. 2–4 were obtained. It is apparent from Fig. 8 that H_3^+ is the dominant ion at all pressures except 1.3 Pa where H_2^+ dominates. However, the H_2^+ flux decreases in intensity with increasing pressure relative to the other ions present in the discharge.

IV. DISCUSSION

Trends in the electrical measurements as the relative concentrations of argon and hydrogen change are associated with changes in the densities and energies of electrons and ions. From Table I it can be seen that as the relative argon content increases, there is a corresponding increase in the fundamental component of the current. This suggests that the ion density in the powered sheath of argon and Ar- H_2 (10%) rf discharges is higher than in pure hydrogen. Additionally, the measured V_b at the powered electrode is 10 V more negative in the Ar- H_2 (10%) mixture than in pure hydrogen. The increase in V_b will give rise to higher mean ion energies at the powered electrode surface as the argon

content increases. Similar measurements at the grounded electrode in the Ar- H_2 (10%) mixture also indicate higher values of the current at the grounded electrode compared to that for pure hydrogen. Furthermore the discharge sheath widths, as evaluated from optical data, are smaller and better defined in pure argon and in Ar- H_2 mixtures than in pure hydrogen.

The observed spectral profiles of H_α emission from discharges, in both pure H_2 and Ar- H_2 mixtures are observed to be symmetric with respect to the central wavelength consistent with previous measurements.¹⁵ The observed wavelength shift in the H_α emission profile for Ar- H_2 mixtures is primarily due to Doppler broadening. Analyses of H_α emission have been made by a number of authors who have studied the dissociation dynamics of the H_2 molecule interacting with a monoenergetic electron beam. Excitation spectra, kinetic energies of dissociation fragments, and Doppler broadening of H_α from electron impact on H_2 have been reported.^{29–33,38,39} It has been shown that not only the kinetic energy and the angular distribution of fragment atoms but also the preferential population of the magnetic sublevels affect the resulting Doppler profiles.⁴⁰

The component of the non-thermal average energy may be calculated upon the assumption that the translational kinetic-energy distribution function of excited hydrogen atoms $f(\epsilon)$ is isotropic and that the line shape $I(\Delta\lambda)$ can be defined as⁴¹

$$I(\Delta\lambda) \propto \int_{\epsilon_{\text{shift}}}^{\infty} \epsilon^{-\frac{1}{2}} f(\epsilon) d\epsilon, \quad (1)$$

where

$$\epsilon_{\text{shift}} = \left(\frac{mc^2}{2} \right) \left(\frac{\Delta\lambda}{\lambda_0} \right)^2 \quad (2)$$

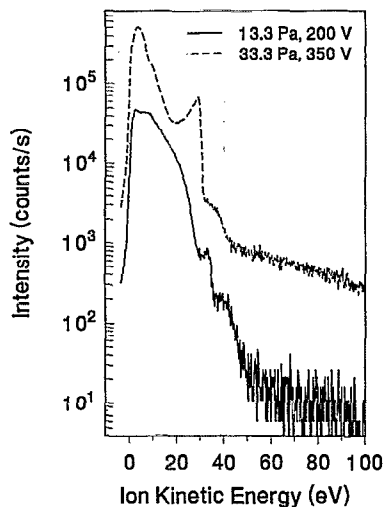


FIG. 7. Kinetic-energy distributions (relative ion intensity versus ion energy) of H^+ ion in Ar- H_2 (10%) discharges at (a) $p=13.3$ Pa and $V_{pp}=200$ V, and (b) $p=33.3$ Pa and $V_{pp}=350$ V.

is the minimum energy of the excited atom for a given Doppler shift $\Delta\lambda$, and λ_0 is the central wavelength, m is the mass of the atom, and c is the speed of light.

In general, optical emission from atoms excited by electron-impact dissociation of H_2 is anisotropic under "beam-like" conditions.^{40,42-44} Because of the randomizing effect of electron-molecule collisions, it is unlikely, however, that the excitation of H_α in the discharge occurs under beam-like conditions. The excitation of H_α directly or indirectly by ion-atom or ion-surface scattering is also not likely to exhibit a high degree of directionality. The H_α emission from the rf discharges in Ar- H_2 (10%) was measured at detection angles of $\theta=80^\circ$ and 90° with respect to the discharge axis. The H_α line profiles at $\theta=80^\circ$ were the same as at 90° consistent with a lack of significant directional anisotropy. A compari-

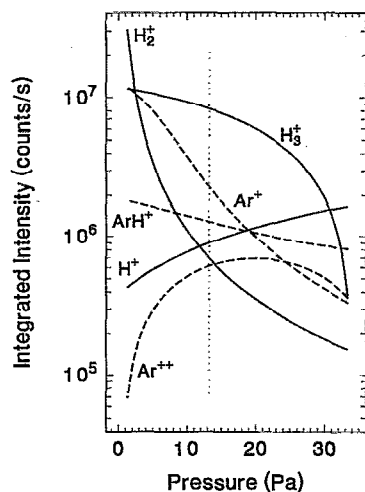


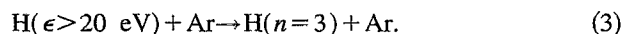
FIG. 8. Integrated ion intensities as a function of pressure in Ar- H_2 (10%), as derived from the IEDs in Figs. 5 and 6.

son of line profiles over a larger range of observation angles would have been preferable but was not possible due to geometrical constraints of the cell.

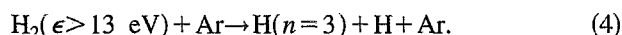
The symmetry of the line profiles and the lack of dependence on the position or direction of observation is consistent with an isotropic distribution of excited-atom velocities. As shown in Fig. 4(a), the phase-resolved optical-emission data for fast H atoms exhibits time variation only near the powered electrode. Although significant Doppler-broadened H_α signal is present throughout the discharge volume, thus indicating the presence of fast atoms, the lack of phase-correlated fluctuations in the signal indicates that the primary ions or atoms have experienced many collisions, which would tend to produce a nearly isotropic distribution of velocities in the bulk of the discharge. The relatively heavy argon atoms are effective in deflecting the hydrogen ions or atoms with little energy loss in recoil.⁴⁵

Since the slow component of the H_α emission results primarily from excitation by electron impact, the spatial-temporal distribution of this emission seen in Fig. 4(b) should be highly correlated with the spatial-temporal variations in the density of electrons with energies in excess of that required for excitation. The results shown in Fig. 4(b) imply that the density of energetic electrons is peaked at the sheath boundary in front of the powered electrode at times when the sheath potential is greatest. By contrast, the intensity of the fast H_α component, as seen in Figs. 3(a) and 4(a), is peaked at the surface of the powered electrode. This is consistent with an excitation process that involves, in the first step, a collision of ions with the electrode. The fact that the fast H_α emission from the mixture extends into the bulk of the plasma is consistent with collisional excitation of fast H neutrals. The shift in temporal phase of the fast component relative to the slow component is also consistent with an excitation process that initially involves ions, since the ion transit times are much longer than electron transit times, and can be comparable to, or greater than, one period of the applied voltage as discussed below.

In the sheath, the Doppler-shifted emission cannot be due primarily to electron collisions with fast H atoms, since calculations show that the electron density in the sheath region should be low.⁴⁶ The emission from the fast H atoms most likely stems from energetic ions or atoms that are formed near or at the powered electrode, and then are able to travel into the discharge volume before being collisionally excited to the $n=3$ state. The increase in Doppler-shifted H_α emission when argon is added to H_2 can be understood from the high excitation cross section for collisions of fast H atoms with argon atoms:³⁷



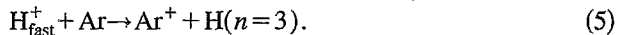
At lower pressures where fast H_2 molecules exist, some contribution from the collisions of these molecules with argon atoms can also be expected:³⁷



It should be noted that emission from fast $H(n=3)$ measured in dc discharges with high electric field-to-gas density ratios (E/N),¹² has been shown to result from fast H atoms collid-

ing with the stationary background gas. The drop off in optical signal from the fast $H(n=3)$ with distance from the powered electrode provides evidence of the loss of energetic neutrals by collisions as they travel through the bulk of the discharge.

The presence of "runaway" ions (see Fig. 7) with kinetic energies comparable to the kinetic energies implied by the Doppler shifts observed in Fig. 2 (≥ 100 eV) suggests that these fast ions contribute to the observed emission via a reaction such as



However, cross sections for this reaction are negligible³⁷ for kinetic energies below 100 eV, and therefore fast H^+ ions cannot be a major direct source of Doppler-broadened emission in the bulk of the plasma. However, the existence of ions with kinetic energies up to 100 eV is consistent with the observed emission profiles (see Fig. 2) in the sense that they provide a source for fast neutrals through collisions with surfaces.

In general, fast atoms have a complex origin and may be produced in the gas phase initially by charge-exchange and neutral-neutral collisions. Fast H atoms may also come from surfaces by dissociation of incident molecular ions, neutralization and scattering of fast ions at the solid surface, ejection of adsorbed hydrogen atoms by ion-surface collisions, and reflection of fast neutrals. In the experiment described here, it was not possible to distinguish these different mechanisms.

The peaks in the time varying emission intensity of Fig. 4(a) provide an indication of when the fast H atoms are formed at the electrode surface. The average translational velocity calculated from the Doppler shift for H atoms with a kinetic energy of 100 eV is 8.8×10^6 cm/s, and the corresponding mean transit time across a 0.5 cm sheath is 57 ns. Average ion transit times can also be calculated using the steady state drift velocity⁴⁷ approximation at $E/N = 2.5 \times 10^{-18}$ V m², which approximates the time-averaged electric fields present in the sheath near the powered electrode at $V_{pp} = 200$ V and $p = 13.3$ Pa. The transit times for H_3^+ ions in argon are estimated to be 185 ns, which is approximately twice the rf period. Meanwhile swarm calculations³⁷ predict runaway for H^+ in Ar for the same E/N value resulting in significantly shorter transit times and higher energies for H^+ than for other ions. Transit times for heavier ions, such as Ar^+ or ArH^+ , in Ar approach 25 rf periods for the same conditions. The fact that a significant time-dependent signal in the optical emission is observed near the powered electrode indicates that the fast H atoms cannot be due primarily to the flux of heavy ions (such as ArH^+) which would be nearly constant in time under these conditions, but result from bombardment by energetic light ions such as H^+ , H_2^+ , and H_3^+ .

Insight into the ion collision processes that are the most likely precursors to formation of fast neutrals can be gained from an interpretation of the observed ion kinetic-energy distributions in light of known collision cross sections.^{37,48-53} Tables III and IV list relevant collision processes along with the region of the discharge in which they would be most

significant, and the cross sections at particular energies of interest. These cross sections apply for a single energy, and are only meant to allow some comparison of relative importance in the discharge. More detailed information about the cross sections can be obtained from the references listed in the tables.

At low pressures, Ar^+ ions are primarily formed by electron-impact ionization (process $i=1$ in Table III) at the bulk-sheath interface. At higher pressures, Ar^+ is formed by charge-transfer collisions in the sheath ($i=2,3$). Charge-transfer processes contribute to the formation of the secondary maxima in the IEDs (see Fig. 5). The IEDs shown in Fig. 5 for Ar^+ ions sampled from the Ar- H_2 (10%) discharges are consistent with our earlier measurements²⁷ in pure argon rf discharges, indicating similar formation processes, i.e., a dominance of process $i=2$. The primary difference between the Ar^+ IEDs in pure argon²⁷ and the mixtures is the large drop in intensity with increasing pressure. This is likely due to additional destruction processes that are the result of collisions of Ar^+ with H_2 . Because of the large mass of Ar^+ relative to H_2 , the exothermic proton transfer leading to the formation of ArH^+ has a large cross section and is one of the dominant processes for Ar^+ destruction ($i=23$). Asymmetric charge-transfer collisions between Ar^+ and H_2 ($i=24$) may also contribute to Ar^+ destruction, but the relative cross sections indicate this process is less significant than ArH^+ formation at the energies of interest here.

The Ar^{++} IEDs have shapes similar to those of Ar^+ , although with much lower intensity. At low pressures, Ar^{++} is formed by high-energy electron impact ($i=4$), while at higher pressures two electron symmetric charge-transfer collisions⁴⁹ may contribute to Ar^{++} formation in the sheath. The formation of the Ar^{++} ions in the sheath result in the formation of the secondary maxima observed in the Ar^{++} IEDs. It should be noted that the formation of Ar^{++} requires electrons with substantial kinetic energies (~ 30 eV).

The discussion of ArH^+ formation published previously²⁷ for "pure" argon discharges is appropriate to the Ar- H_2 mixture studied here, except that the increased concentration of H_2 may make some additional reactions relevant, for example, reactions involving H_2^+ and H_3^+ . At low pressures, ArH^+ is formed predominately in the bulk region by low-energy collisions between Ar^+ and H_2 or H_2^+ and Ar ($i=6,7$). The secondary maxima observed in the ArH^+ IEDs at higher pressures indicates contributions to formation of ArH^+ ions by higher energy ion-molecule collisions in the sheath region ($i=8-10$). Destruction of ArH^+ ions by collisions with neutral Ar and H_2 may be important in the sheath regions, but the cross sections and resultant products for these processes are not known.

The ions Ar^+ and Ar^{++} could be a source of fast H atoms through desorption of adsorbed hydrogen on the surface of the electrodes, and ArH^+ could conceivably be a source of fast H atoms by dissociation and backscattering of products following bombardment of the powered electrode surface. However, as noted above, the observed time-dependent variation of the optical emission (Fig. 4) requires that the primary source of fast H atoms observed here be

TABLE III. Possible ion formation processes in the Ar-H₂ mixtures in the rf discharges. The cross sections apply at the specific energies indicated.

<i>i</i>	Excitation region	Reaction	Cross section (m ²)	Energy (eV)	Ref.
Ar⁺					
1	Bulk-sheath edge	Ar + e → Ar ⁺ + 2e	1.7 × 10 ⁻²⁰	50	51
2	Sheath	Ar ⁺ + Ar → Ar + Ar ⁺	4 × 10 ⁻¹⁹	10	50
3	Sheath	H ₃ ⁺ + Ar → Ar ⁺ + H ₂ + H	3 × 10 ⁻²⁰	10	37
Ar²⁺					
4	Bulk-sheath edge	Ar + e → Ar ²⁺ + 3e	4.9 × 10 ⁻²²	50	52
5	Sheath	Ar ²⁺ + Ar → Ar + Ar ²⁺	8.7 × 10 ⁻²⁰	20	49
ArH⁺					
6	Bulk	H ₂ ⁺ + Ar → ArH ⁺ + H	2.4 × 10 ⁻¹⁹	0.5	37
7	Bulk	Ar ⁺ + H ₂ → ArH ⁺ + H	5.5 × 10 ⁻¹⁹	0.5	37
8	Sheath	H ₂ ⁺ + Ar → ArH ⁺ + H	2.6 × 10 ⁻²⁰	10	37
9	Sheath	H ₃ ⁺ + Ar → ArH ⁺ + H ₂	1.3 × 10 ⁻²⁰	10	37
10	Sheath	Ar ⁺ + H ₂ → ArH ⁺ + H	1.4 × 10 ⁻¹⁹	20	37
H⁺					
11	Bulk-sheath edge	H ₂ + e → H ⁺ + H + 2e	1 × 10 ⁻²²	40	53
12	Sheath	H ₂ ⁺ + Ar → H ⁺ + H + Ar	1 × 10 ⁻²²	10	37
13	Sheath	H ₃ ⁺ + H ₂ → H ⁺ + H ₂ + H	8.5 × 10 ⁻²¹	10	48
14	Sheath	H ⁺ + H → H + H ⁺	4.0 × 10 ⁻¹⁹	10	48
15	Sheath	Ar ⁺ + H ₂ → H ⁺ + H + Ar	2.5 × 10 ⁻²¹	100	37
H₂⁺					
16	Bulk-sheath edge	H ₂ + e → H ₂ ⁺ + 2e	9 × 10 ⁻²¹		53
17	Sheath	Ar ⁺ + H ₂ → H ₂ ⁺ + Ar	9 × 10 ⁻²¹	10	37
18	Sheath	H ₂ ⁺ + H ₂ → H ₂ + H ₂ ⁺	1.1 × 10 ⁻¹⁹	10	48
19	Sheath	H ⁺ + H ₂ → H ₂ ⁺ + H	5.4 × 10 ⁻²¹	10	48
H₃⁺					
20	Bulk	H ₂ ⁺ + H ₂ → H ₃ ⁺ + H	3 × 10 ⁻¹⁹	0.5	48
21	Sheath	ArH ⁺ + H ₂ → H ₃ ⁺ + Ar			37
22	Sheath	H ₂ ⁺ + H ₂ → H ₃ ⁺ + H	4 × 10 ⁻²¹	10	48

TABLE IV. Possible ion destruction processes in the Ar-H₂ mixtures in the rf discharges. The cross sections apply at the specific energies indicated.

<i>i</i>	Excitation region	Reaction	Cross section (m ²)	Energy (eV)	Ref.
Ar⁺					
23	Sheath	Ar ⁺ + H ₂ → ArH ⁺ + H	1.8 × 10 ⁻¹⁹	10	37
24	Sheath	Ar ⁺ + H ₂ → Ar + H ₂ ⁺	7.6 × 10 ⁻²⁰	10	37
ArH⁺					
25	Sheath	ArH ⁺ + H ₂ → H ₃ ⁺ + Ar			
26	Sheath	ArH ⁺ + Ar → Ar ⁺ + ArH			
H⁺					
27	Bulk	H ⁺ + H ₂ + M → H ₃ ⁺ + M			48
28	Sheath	H ⁺ + Ar → Ar ⁺ + H	3 × 10 ⁻²⁴	40	37
29	Sheath	H ⁺ + H ₂ → H ₂ ⁺ + H	3 × 10 ⁻¹⁹	10	48
H₂⁺					
30	Bulk	H ₂ ⁺ + Ar → ArH ⁺ + H	2.4 × 10 ⁻¹⁹	0.5	37
31	Sheath	H ₂ ⁺ + H ₂ → H ₃ ⁺ + H	2.4 × 10 ⁻¹⁹	10	48
32	Sheath	H ₂ ⁺ + Ar → Ar ⁺ + H ₂	4 × 10 ⁻²⁰	10	37
33	Sheath	H ₂ ⁺ + H ₂ → H ⁺ + H ₂ + H	8.5 × 10 ⁻²¹	10	48
34	Sheath	H ₂ ⁺ + Ar → H ⁺ + H + Ar	5.5 × 10 ⁻²¹	10	37
H₃⁺					
35	Sheath	H ₃ ⁺ + Ar → ArH ⁺ + H ₂	1.3 × 10 ⁻²⁰	10	37
36	Sheath	H ₃ ⁺ + H ₂ → H ₂ ⁺ + H + H ₂	5.5 × 10 ⁻²²	20	48

associated with surface bombardment by fast, light species, such as H^+ , H_2^+ , and H_3^+ . In general, the IEDs of ions from hydrogen (Fig. 6) differ substantially from those of ions from argon because their light mass and subsequently shorter transit times in the sheath. Because the average transit time of these ions are comparable to the period of the applied rf excitation voltage, their kinetic energy can approach the maximum allowed by the plasma (sheath) potential.

Dissociative ionization by electron impact of H_2 ($i=11$) and dissociative charge exchange between H_2^+ and H_2 or Ar ($i=12,13$) are the primary reactions responsible for the production of H^+ in the bulk and in the sheath of the discharge, respectively. Dissociative charge exchange between high energy (≥ 100 eV) Ar^+ ions and H_2 ($i=15$) may be a source of H^+ at the powered electrode, but not for the IEDs measured here at the grounded electrode. Destruction of H^+ occurs through asymmetric charge-transfer collisions with argon and H_2 in the sheath region ($i=28,29$), and by low-energy three-body collisions in the bulk to form H_3^+ ($i=27$). From Figs. 6 and 8, it is evident that the flux of H^+ ions at the grounded electrode increases with pressure relative to the other ions. This may be primarily due to an increase in the frequency of the collisions that result in the formation of H^+ via the destruction of H_2^+ ($i=12,13$).

The H_2^+ ion predominates in the discharge at 1.3 Pa where the primary source is ionization of H_2 by electron impact ($i=16$). At higher pressures, asymmetric charge transfer of Ar^+ with H_2 ($i=17$), and symmetric charge-exchange collisions with H_2 ($i=18$) make a greater contribution to H_2^+ formation in the sheath region. Formation of H_2^+ by asymmetric charge transfer of H^+ with H_2 ($i=19$) also contributes, but at a lower rate due to a smaller cross section as compared to reactions 17 and 18. Although, the destruction mechanisms for H_2^+ are numerous ($i=30-34$), the predominate loss process in the Ar- H_2 mixture is likely to be the proton-transfer reaction which leads to the formation of ArH^+ . The cross section for this process is largest at thermal energies, but remains significant for energies up to 10 eV. Other processes involve the conversion to H_3^+ at low energies in the plasma bulk, and conversion to Ar^+ and H^+ at higher energies in the sheath. The drop in relative H_2^+ intensity with increasing pressure evident in Fig. 8 is a result of the increasing probability of the collisions that destroy this ion.

The H_3^+ ions are predominantly produced in the bulk of the discharge by a proton-exchange reaction and then accelerated by the sheath field, where they experience little energy loss due to collisions. If sufficient hydrogen is present in the mixture, ArH^+ and H_2^+ ions will react with hydrogen molecules at relatively high energies in the sheath to produce H_3^+ ($i=21,22$). These reactions are undoubtedly responsible for the secondary structure evident in the H_3^+ IEDs at higher pressures. Destruction mechanisms for H_3^+ ($i=35,36$) are dominated by collisions with Ar to form ArH^+ .

V. CONCLUSIONS

From Fig. 8, it is evident that at the pressure used to obtain the optical data (13.3 Pa), H_3^+ is the dominant light

ion with H^+ and H_2^+ having intensities more than ten times lower. Additionally, from Fig. 6 it is evident that H_3^+ has the highest mean energy of the ions, even though H^+ exhibits the highest maximum kinetic energies. These observations suggest that H_3^+ is the primary source of fast H emitted from the surface of the powered electrode. This conclusion requires that the gas-phase destruction mechanisms for H_3^+ should not significantly increase at the higher ion kinetic energies that can be produced by acceleration across the sheath near the powered electrode, as compared to the energies gained in the sheath near the grounded electrode. This seems unlikely since none of the destruction mechanisms listed in Table IV exhibit a significant energy dependence over the range of 10–200 eV. An additional consideration is the relative yield of fast H atoms due to bombardment of a surface by fast H_3^+ ions. At present, no experimental data exists on the breakup of H_3^+ upon striking aluminum surfaces.

The H^+ ion cannot be ruled out as an additional source of fast H atoms. At the high ion energies observed here, fast H atoms are known to be formed by bombardment of surfaces by H^+ .⁵⁴ A significant contribution from H_2^+ is unlikely, due to the very fast conversion of H_2^+ to H_3^+ , especially at higher pressures.

ACKNOWLEDGMENT

The authors would like to thank Mark Sobolewski for his help in performing the current and voltage measurements.

- ¹Y. Aoki, S. Aoyama, H. Uetake, K. Morizuka, and T. Ohmi, *J. Vac. Sci. Technol.* **11**, 307 (1993).
- ²H. Tsai and D. B. Bogy, *J. Vac. Sci. Technol. A* **5**, 3287 (1987).
- ³M. Baer and H. Nakamura, *J. Chem. Phys.* **87**, 4651 (1987).
- ⁴P. J. Kuntz and A. C. Roach, *J. Chem. Soc. Faraday Trans. II* **68**, 259 (1972).
- ⁵S. Chapman and R. K. Preston, *J. Chem. Phys.* **60**, 650 (1974).
- ⁶S. Chapman *J. Chem. Phys.* **82**, 4033 (1985).
- ⁷M. Baer and J. A. Beswick, *Chem. Phys. Lett.* **51**, 360 (1977).
- ⁸M. Baer and J. A. Beswick, *Phys. Rev. A* **19**, 1559 (1979).
- ⁹M. Baer, H. Nakamura, and A. Ohsaki, *Chem. Phys. Lett.* **131**, 468 (1986).
- ¹⁰M. Baer and H. Nakamura, *J. Phys. Chem.* **91**, 5503 (1987).
- ¹¹C. Y. Ng and M. Baer, *State Selected and State to State Ion-Molecule Dynamics Part* (Wiley, New York, 1992).
- ¹²B. M. Jelenkovic, Z. Lj. Petrovic, and A. V. Phelps, 1990 Gaseous Electronics Conference Abstracts, p. 170.
- ¹³M. Kuraica and N. Konjevic, *Phys. Rev. A* **46**, 4429 (1992).
- ¹⁴M. Kuraica, N. Konjevic, and M. Platasa, *Spectrochim. Acta Part B* **47**, 1173 (1992).
- ¹⁵S. Djurovic and J. R. Roberts, *J. Appl. Phys.* **74**, 11 (1994).
- ¹⁶D. Field, D. F. Klemperer, P. W. May, and Y. P. Song, *J. Appl. Phys.* **70**, 82 (1991).
- ¹⁷A. D. Kuypers and H. J. Hopman, *J. Appl. Phys.* **67**, 1229 (1990).
- ¹⁸A. Manenschijn, G. C. A. M. Janssen, E. van der Drift, and S. Radelaar, *J. Appl. Phys.* **69**, 1253 (1991).
- ¹⁹J. K. Olthoff, R. J. Van Brunt, S. B. Radovanov, and J. A. Rees, *IEE Proc.-Sci. Meas. Technol.* **141**, 105 (1994); J. K. Olthoff, R. J. Van Brunt, and M. A. Sobolewski, in *Proceedings of the Tenth International Conference on Gas Discharges and their Applications*, edited by W. T. Williams (University College of Swansea, Swansea, Wales, 1992), Vol. 1, p. 440.
- ²⁰W. Benesh and E. Li, *Opt. Lett.* **9**, 338 (1984); E. Li, Ayers and W. Benesh, *Phys. Rev. A* **37**, 194 (1988); C. Barbeau and J. Jolly, *J. Phys. D* **23**, 1168 (1990); S. A. Bzenic, S. B. Radovanov, S. B. Vrhovac, Z. B. Velikic, and B. M. Jelenkovic, *Chem. Phys. Lett.* **184**, 108 (1991); G. Sultan, G. Baravian, M. Gantois, G. Henrion, H. Michel, and A. Ricard, *Chem. Phys.* **123**, 423 (1988); A. L. Cappelli, R. A. Gottscho, and T. A. Müller, *Plasma Chem. Plasma Proc.* **5**, 317 (1985); G. Baravian,

- Y. Chouan, A. Ricard, and J. Sultan, *J. Appl. Phys.* **61**, 5249 (1987); S. V. Vrhovac, S. B. Radovanov, S. A. Bzenic, Z. Lj. Petrovic, and B. M. Jelenkovic, *Chem. Phys.* **153**, 233 (1991).
- ²¹F. Tochikubo, T. Kokubo, S. Kakuta, A. Suzuki, and T. Makabe, *J. Phys. D* **23**, 1184 (1990); F. Tochikubo, A. Suzuki, S. Kakuta, Y. Terazono, and T. Makabe, *J. Appl. Phys.* **68**, 5532 (1990); F. Tochikubo, T. Makabe, S. Kakuta, and A. Suzuki, *ibid.* **71**, 2143 (1992); F. Tochikubo and T. Makabe, *Meas. Sci. Technol.* **2**, 1133 (1991).
- ²²Z. Lj. Petrovic, B. M. Jelenkovic, and A. V. Phelps, *Phys. Rev. Lett.* **68**, 325 (1992).
- ²³P. J. Hargis, K. E. Greenberg, P. A. Miller, J. B. Gerardo, J. R. Torczynski, M. E. Riley, G. A. Hebner, J. R. Roberts, J. K. Olthoff, J. R. Whetstone, R. J. Van Brunt, M. A. Sobolewski, H. A. Anderson, M. P. Splichal, J. L. Mock, P. Bletzinger, A. Garscadden, R. A. Gottscho, G. Selwyn, M. Dalvie, J. E. Heidenreich, J. W. Butterbaugh, M. L. Brake, M. L. Passow, J. Pender, A. Lujan, M. E. Elta, D. B. Gravcs, H. H. Sawin, M. J. Kushner, J. T. Verdeyen, R. Horwath, and T. R. Turner, *Rev. Sci. Instrum.* **65**, 140 (1994).
- ²⁴M. A. Sobolewski, *J. Vac. Sci. Technol. A* **10**, 3550 (1992).
- ²⁵P. A. Miller, H. A. Anderson, and M. P. Splichal, *J. Appl. Phys.* **71**, 1171 (1992).
- ²⁶J. K. Olthoff, S. B. Radovanov, and R. J. Van Brunt, *Appl. Phys. Lett.* (in press).
- ²⁷J. K. Olthoff, R. J. Van Brunt, S. B. Radovanov, J. A. Rees, and R. Surowiec, *J. Appl. Phys.* **75**, 115 (1994); J. K. Olthoff, R. J. Van Brunt, and S. B. Radovanov, *ibid.* **72**, 4566 (1992).
- ²⁸S. Djurović, J. R. Roberts, M. A. Sobolewski, and J. K. Olthoff, *J. Res. Natl. Inst. Stand. Technol.* **98**, 159 (1993).
- ²⁹R. S. Freund, J.A. Chiavone, and D. F. Brader, *J. Chem. Phys.* **64**, 1122 (1976).
- ³⁰K. Ito, N. Oda, Y. Hatano, and T. Tsuboi, *Chem. Phys.* **17**, 35 (1976).
- ³¹G. N. Polyakova, V. F. Erko, A. I. Ranynk, and O. S. Pavlichenko, *Sov. Phys.-JETP* **44**, 921 (1976).
- ³²M. Glass-Maujean, *J. Phys. B: At. Mol. Phys.* **11**, 431 (1978).
- ³³T. Ogawa and M. Higo, *Chem. Phys.* **52**, 55 (1980).
- ³⁴K. Köhler, J. W. Coburn, D. E. Horne, and E. Kay, *J. Appl. Phys.* **57**, 59 (1985).
- ³⁵Ch. Wild and P. Koidl, *J. Appl. Phys.* **68**, 6125 (1990).
- ³⁶R. T. C. Tsui, *Phys. Rev.* **168**, 107 (1968).
- ³⁷A. V. Phelps, *J. Phys. Chem. Ref. Data* **21**, 883 (1992).
- ³⁸F. J. de Heer, H. A. van Sprang, and G. R. Mohlmann, *J. Chem. Phys.* **77**, 773 (1980).
- ³⁹N. Kouchi, K. Ito, Y. Hatano, and N. Oda, *Chem. Phys.* **70**, 105 (1982).
- ⁴⁰R. J. Van Brunt and R. N. Zare, *J. Chem. Phys.* **48**, 4304 (1968).
- ⁴¹M. Higo and T. Ogawa, *Chem. Phys.* **44**, 279 (1979).
- ⁴²J. Kurawaki and T. Ogawa, *Chem. Phys. Lett.* **98**, 12 (1983).
- ⁴³R. H. McFarland and E. A. Soltysik, *Phys. Rev. A* **129**, 2581 (1963).
- ⁴⁴N. Takahashi, S. Arai, N. Kouchi, N. Oda, and Y. Hatano, *J. Phys. B: At. Mol. Phys.* **16**, L547 (1983).
- ⁴⁵E. W. McDaniel, *Collision Phenomena in Ionized Gases* (Wiley, New York, 1964).
- ⁴⁶B. Chapman, *Glow Discharge Processes* (Wiley, New York, 1980); D. Field, D. F. Klemperer, P. W. May, and Y. P. Song, *J. Appl. Phys.* **70**, 82 (1991); J. A. Stratton, *Electromagnetic Theory* (McGraw-Hill, New York, 1941); J. L. Delcroix, *Plasma Physics* (Wiley, New York, 1965).
- ⁴⁷B. Van Zyl, H. Neuman, H. L. Rothwell, and R. C. Amme, *Phys. Rev. A* **21**, 716 (1980).
- ⁴⁸A. V. Phelps, *J. Phys. Chem. Ref. Data* **19**, 653 (1990).
- ⁴⁹A. V. Phelps, *J. Appl. Phys.* **76**, 747 (1994).
- ⁵⁰A. V. Phelps, *J. Chem. Phys. Ref. Data* **20**, 557 (1991).
- ⁵¹J. E. Lawler, *Phys. Rev. A* **32**, 2977 (1985); A. V. Phelps and B. M. Jelenkovic, *ibid.* **38**, 2975 (1988); D.A. Scott and A. V. Phelps, *ibid.* **43**, 3043 (1991).
- ⁵²L. J. Kieffer and G. H. Dunn, *Rev. Mod. Phys.* **38**, 1 (1966).
- ⁵³H. Tawara, Y. Itakawa, Y. Itoh, H. Nishimura, S. Ohtani, H. Takagi, K. Takayanagi, and M. Yoshino, *Atomic Data Involving Hydrogens Relevant to Edge Plasmas*, Report IPPJ-AM-46, 41 (1986).
- ⁵⁴G. M. Cracken, *Rep. Prog. Phys.* **38**, 241 (1975).